Green Chemistry

PAPER

View Article Online
View Journal | View Issue

Cite this: *Green Chem.*, 2021, **23**, 6036

Integration of acetic acid catalysis with one-pot protic ionic liquid configuration to achieve high-efficient biorefinery of poplar biomass†

Kaixuan Huang,[a,b,c,d] Mood Mohan,[b,e] Anthe George,[b,e] Blake A. Simmons,[b,c] Yong Xu*[a] and John M. Gladden*[b,e]

Recyclable biocatalysts and high-efficiency lignocellulose deconstruction are the crucial factors for cost-effective conversion of biomass into biofuels and bioproducts. Acetic acid-based catalytic hydrolysis of grassy lignocellulosic biomass presents a promising application because of its effectivity, recyclability, and other environmentally friendly features. However, this treatment is not as effective on woody biomass, such as poplar. One way to improve conversion performance of this process is to integrate it with other effective processes, such as pretreating biomass with protic ionic liquids (PILs) that have been shown to effectively solubilize lignin in reducing the recalcitrance of biomass to enzymatic deconstruction. In this work, an integrated acetic acid based one-pot ethanolamine acetate pretreatment (HAc–[EOA][OAc]) was developed for the efficient depolymerization of poplar polysaccharides. The configuration simultaneously removed ~88% hemicellulose and selectively extracted up to ~46% of the lignin from lignocellulosic biomass. HAc–[EOA][OAc] pretreated poplar yielded over 80% enzyme-hydrolyzed glucose that was attributed to an increase in the accessible surface area of cellulose to the hydrolytic enzymes. Analysis of the cellulose crystallinity and thermal decomposition profiles revealed that all pretreated samples have a higher cellulose crystallinity, indicating that amorphous cellulose had been removed during pretreatment. Conductor like screening model for real solvents (COSMO-RS) and Hansen solubility parameters (HSP) were used to provide insights into the mechanism of biomass pretreatment efficacy using both HAc and [EOA][OAc]. We found that a strong hydrogen-bonding and electrostatic misfit interaction between hemicellulose and HAc may explain the higher removal of hemicellulose during HAc pretreatment. Further, the close HSP values and COSMO-RS analysis indicate that [EOA][OAc] is a good lignin solvent, which leads to the higher delignification of biomass. This study demonstrates that the integration of IL with acid pretreatment is a promising strategy for conducting effective pretreatment on woody lignocellulose.

Received 15th May 2021,
Accepted 25th June 2021

DOI: 10.1039/d1gc01727f

rsc.li/greenchem

1. Introduction

Given the widespread availability and sustainability of non-food plant biomass, it is a promising carbon source for the production of renewable alternatives to fossil fuels. The efficient breakdown of lignocellulose into functional molecules is the major hurdle limiting the establishment of economical lignocellulosic biorefineries.[1] To reduce the recalcitrant lignocellulosic biomass to enzymatic deconstruction, researchers have attempted to develop the affordable and scalable biomass pretreatment approaches that can effectively enable conversion to biofuels and value-added chemicals.[2,3]

Several pretreatment techniques have been studied over the past few years, such as steam explosion, hot water, dilute mineral acids, organic acids, and ammonia-based.[4] Pretreatment with acetic acid (HAc) has proven to be a promising method compared to some other deconstruction techno-

[a]*Key Laboratory of Forestry Genetics & Biotechnology (Nanjing Forestry University), Ministry of Education, Nanjing 210037, People's Republic of China. E-mail: xuyong@njfu.edu.cn*
[b]*Joint BioEnergy Institute, 5885 Hollis Street, Emeryville, California 94608, USA. E-mail: jmgladden@lbl.gov*
[c]*Biological Systems and Engineering Division, Lawrence Berkeley National Laboratory, 1 Cyclotron Road, Berkeley, California 94720, USA*
[d]*College of Marine and Bio-engineering, Yancheng Teachers University, Yancheng, Jiangsu 224002, People's Republic of China*
[e]*Biomass Science and Conversion Technology, Sandia National Laboratories, 7011 East Avenue, Livermore, California 94551, USA*

†Electronic supplementary information (ESI) available: Quantum chemical-based predicted favorability of proton transfer between acid and base, interaction energies between molecular species of acid and base and ionic species of anion and cation of IL, NMR, TGA/DTG analysis of [EOA][OAc], cartesian coordinates (in Å) of isolated molecules of neutral and ionic species, cartesian coordinates (in Å) and calculated lowest energy conformers of lignin-amine/organic solvent complexes, cartesian coordinates (in Å) of cellulose, hemicellulose, and lignin. See DOI: 10.1039/d1gc01727f

logies. It can efficiently depolymerize hemicellulose (from poplar fibers) into sugars (xylose, arabinose, *etc.*) and oligosaccharides with recyclable catalysts and render cellulose more amenable to cellulolytic enzyme.[5,6] A HAc-based integrated process that combines biomass pretreatment and enzymatic hydrolysis can be efficiently scaled-up and potentially attain commercial viability. However, there remain some challenges related to hexose release during the saccharification of HAc pretreated poplar that needs to be addressed prior to the fulfillment of comprehensive utilization of woody biomass. Our previous study demonstrated that after the deconstruction of hemicellulose using HAc, it is possible to increase the enzymatic efficiency of cellulose 1.8-fold compared with its counterpart after autohydrolysis pretreatment.[6] Despite this exciting advance, the fermentable sugar yield is insufficient for efficient biofuel production. The higher degree of cellulose crystallinity and lignin content represent the dominant factors contributing to the lower hydrolysis rates of the HAc refined cellulosic substrate.[2,7,8] In this regard, due to the difficulty to deconstruct the cellulosic poplar structure after HAc pretreatment, it will need to be integrated with techniques that can effectively disrupt the cellulose structures and solubilize lignin, such as ionic liquid (IL) pretreatment.[9,10]

Among the various classes of ILs, protic ILs (PILs) are easily derived from mixing a Brønsted acid with a Brønsted base that permit a proton transfer and generation of ions.[11,12] PILs also possess similar properties as aprotic ILs such as low vapor pressure, high ionic conductivity, high chemical and thermal stability, and low flammability. PILs have shown versatile applications in biomass pretreatment and several were demonstrated to have the ability to delignify several types of biomass through their solvent–substrate interactions.[8,13–15] The preparation of PILs is simple, cheap, and commercially viable compared to traditional imidazolium-based ILs. Several PILs have also been shown to be biocompatible and permit the function of both enzymes and microbes.[8] Moreover, PILs can be distilled at low pressure without decomposition and are volatilized as neutral molecular species by a reverse proton transfer mechanism. This characteristic can therefor enable distillation-based IL recycling.[16] Given the potential of PILs, ethanolamine acetate ([EOA][OAc]) has proven to be effective for biomass pretreatment, especially when it was implemented on one-pot pretreatment of grassy feedstocks.[8] In another study with switchgrass, a satisfactory yield of glucose (~85%) was achieved after [EOA][OAc] pretreatment at 160 °C for 0.5 h, which has been shown that PIL can be the potential solvent in disruption of the inter- and intra-molecular hydrogen bonding in cellulose.[17] Very recently, Zhou *et al.* studied the delignification effect of *Miscanthus x giganteus* using [EOA][OAc] and reported that this PIL has an excellent ability to delignify the biomass.[18]

Based on this superior performance, it is expected that biomass pretreatment using [EOA][OAc] may also positively impact the crystallinity of cellulose in hardwood (*e.g.* poplar). In addition, it was also reported that [EOA][OAc] can address the issue of pH compatibility in an integrated biomass-to-biofuel configuration since this PIL results in a slightly acidic pH after pretreatment, which is compatible with downstream lignocellulose-deconstructing enzymes.[8] In this case, the pH compatibility reduces process complexity and cost associated with reagents required for pH adjustment as is the case with more basic PILs. Importantly, studies have also shown that lignocellulose-deconstructing enzyme cocktails can tolerate 10 wt% loading of PIL during the saccharification process, thus avoiding the need for water-wash or solid/liquid separation steps after pretreatment.[19] In addition, the biocompatibility of PIL with microorganisms (*e.g. Saccharomyces cerevisiae*) was also demonstrated.[8] With such advancements, by combining acid hydrolysis and one-pot PIL unit operations (pretreatment and saccharification), the new consolidated process allows high sugar conversion and enables a cost-competitive biorefinery.

In this work, for the first time, we report the integration of acetic acid and ionic liquid pretreatments to achieve a high level of depolymerization of polysaccharides from woody biomass (Fig. 1). In our previous studies, we have optimized the maximum hemicellulose removal and produced value-added chemicals using acetic acid pretreatment with minimal effect on cellulose and lignin.[6] Here, biomass was pretreated and then enzymatically hydrolyzed using a one-pot PIL strategy to increase the efficiency of monomeric sugar release. Furthermore, the effect of water content on PIL biomass pretreatment was also investigated to verify the possibility of potentially using less PIL in the process. Different process scenarios were investigated to integrate the acid hydrolysis with the one-pot PIL pretreatment to identify the optimal strategy. Finally, since the mechanism of lignin solubilization during biomass pretreatment using [EOA][OAc] is not well understood, we computationally evaluated the interactions between [EOA][OAc] and individual lignocellulosic compounds using COSMO-RS (conductor like screening model for real solvents) and Hansen solubility parameters. It is believed that the integrated technology introduced here could provide woody biorefineries with a promising route to achieve a sustainable bioeconomy. In the present study, the motivation for [EOA][OAc] selection is that it is recoverable, easy to prepare, cheaper, and a promising IL for biomass pretreatment.

2. Results and discussion

2.1 Individual *vs.* consolidated pretreatment and saccharification

An individual HAc catalytic hydrolysis of poplar achieved a yield of 51.4% xylooligosaccharides (DP 2–10), which was lower than observed with grasses.[6,20] As expected, the sugar yields of glucose (57.1%) and xylose (61.7%) obtained after 72 h of enzymatic saccharification were relatively low. To overcome this barrier, one-pot pretreatment and saccharification using [EOA][OAc] was evaluated on biomass residues resulting from HAc-catalyzed poplar (ACP) treatment, with untreated

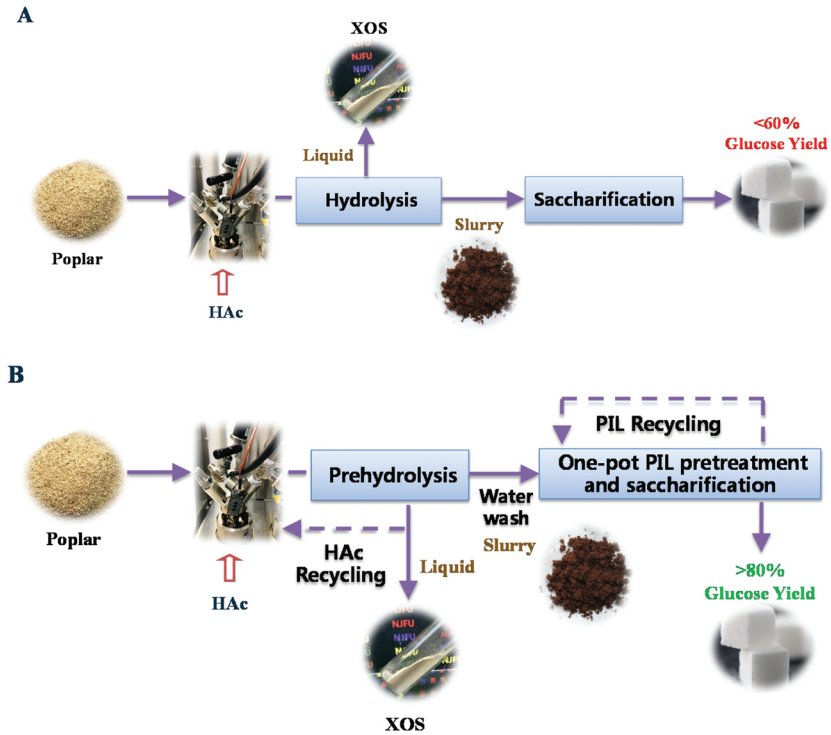

Fig. 1 Process design differences between HAc and HAc–[EOA][OAc] pretreatment. (A) A previous HAc-based strategy for sugar release. (B) A consolidated and intensified process for optimal HAc–[EOA][OAc] conditions to pretreat poplar.

poplar as a control. Results from a side-by-side comparison of sugar yields liberated from ACP during pretreatment and saccharification (consolidated pretreatment) for each of two process scenarios (pH adjustment and water wash) are reported in Fig. 2. The pH adjustment (pH ~ 7) in [EOA][OAc]-based integrated process resulted in 65.9% glucose and 62.2% xylose yields based on the digestible polysaccharide-enriched solids after the saccharification step, which in terms of glucose and xylose yields are lower than the water-wash process (83% glucose and 74.8% xylose). The result without pH adjustment was better than using NaOH for neutralization. This could be attributed to the aggregation effect occurring on the enzyme surface upon contact with salt molecules.[21] Based on these results, the water-wash scenario was selected for further investigation for the development of a one-pot strategy. Recently, Mohan *et al.* reported the consolidated pretreatment

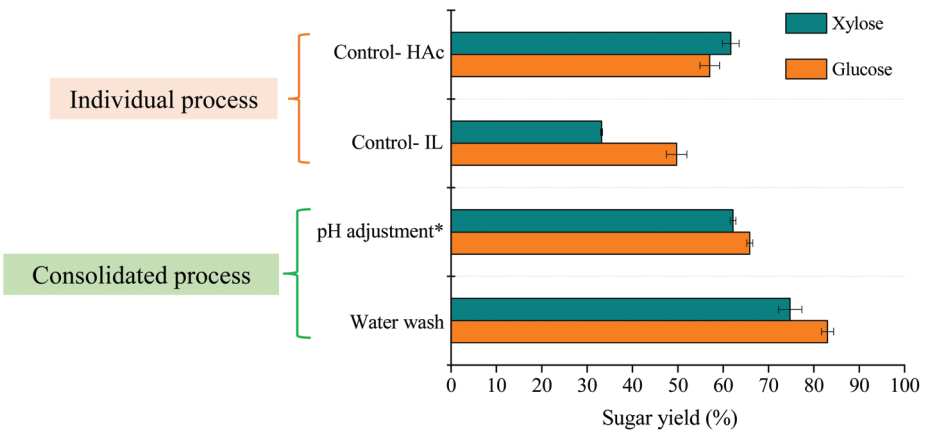

Fig. 2 Comparisons of impacts of individual and consolidated pretreatments on enzymatic hydrolysis. Conditions: pretreatment, 20 wt% ACP loading, 80 wt% IL, 140 °C, 3 h; saccharification, 10 wt% IL, 2.5% solid loading, 20 mg protein per g ACP, 50 °C, 72 h. *: pH was adjusted to 7.0 with 2 M NaOH solution.

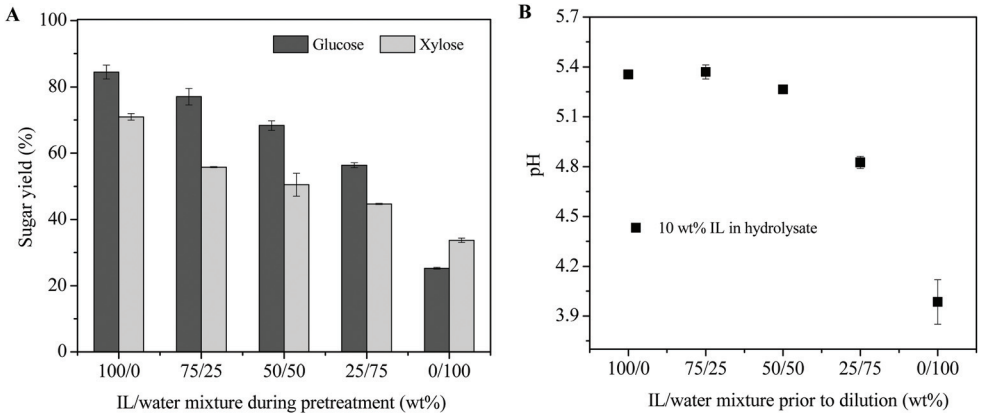

Fig. 3 (A) Effects of water concentration during IL solvation on ACP for sugar release. Conditions: pretreatment, 20 wt% ACP loading, 0–80 wt% IL, 140 °C, 3 h; saccharification, 10 wt% IL, 20 mg protein per g ACP, 50 °C, 72 h. (B) 10 wt% IL in the hydrolysate.

of bamboo in H_2SO_4-[C_2C_1Im][OAc] (*i.e.*, acid pretreatment followed by IL pretreatment) to understand the effect of the consolidated process on reducing sugars yield.[22] A glucose yield of 90% was achieved after enzymatic hydrolysis. However, a low solid loading (1.3 wt%) and a high enzyme loading (50 mg of cellulase (ATCC 26921) enzyme) were used, so the results may not be reflective of a more intensified process that would be required for a sustainable biorefinery. The implementation of sulfuric acid, [C_2C_1Im][OAc] IL, lower biomass loading, and higher enzyme loading results in higher biorefinery process cost. Therefore, in our case, the higher solid loading (2.5 wt%), lower enzyme amount (20 mg protein per g biomass), and cheaper PIL were used in order to minimize the capital costs.

Previous studies have reported that comparable sugar yields can be obtained using lower IL concentrations (10–50 wt%) for certain ILs, such as 1-ethyl-3-methylimidazolium acetate ([C_2mim][OAc]) and cholinium lysinate ([Ch][Lys]).[9,10] Using an aqueous mixture of IL as a pretreatment solvent is more favorable for an industrial application due to viscosity reduction, minimal energy input and costs, and the lack of dilution of the IL-slurry post-pretreatment, which simplifies IL recovery.[10] To evaluate the potential of PIL–H_2O mixtures, we compared sugar yields from one-pot pretreatment of ACP (20 wt% loading) at different water concentrations (0–100 wt% in IL/water mixture). Pretreatment with pure IL (0% water) yielded the highest sugar release after saccharification while increasing water concentrations led to lower sugar yields (Fig. 3). It has been reported that the presence of water could weaken the solvation ability of IL on biomass and it acts as an anti-solvent.[23,24] Therefore, the presence of water reduced the efficiency of IL pretreatment of biomass which resulted in lower sugar release. Meanwhile, the pH value of PIL (10 wt% in hydrolysate) is in a mildly acidic pH range ~4.8–5.4, which is suitable for commercially available lignocellulose-degrading enzymes. This data is in agreement with the literature and the fact that [EOA][OAc] is a pH compatible and biocompatible IL, suggests that it could be used in a one-pot process.[8] It is also worthwhile to mention that the use of anhydrous PIL might increase the capital or utility cost.

2.2 Variables impacting PIL performance during one-pot pretreatment and saccharification

Sugar yields from [EOA][OAc]-pretreated ACP (EA-ACP) can be affected by pretreatment parameters (*e.g.* biomass to IL weight ratio, temperature, and time) and saccharification parameters (*e.g.* IL concentration and enzyme loading). Thus, the influence of these parameters on sugar production was investigated in an attempt to maximize efficiency (Fig. 4). Based on the previous investigation, [EOA][OAc] possesses a superb capacity for 20 wt% biomass loading for pretreatment.[8] Therefore, we also investigated the impact of higher biomass loadings, from 20 to 50 wt% (Fig. 4A). It was seen that increasing the biomass loading from 20 to 40 wt% resulted in a minor difference in the glucose yields (more than 70%) and the similar yields of xylose. Further increasing the biomass loading to 50 wt% resulted in a significant reduction in glucose and xylose yields. On the other hand, variation of temperature and time seemed to greatly affect fermentable sugar release during enzymatic saccharification. From Fig. 4B, an elevation of temperature (120 to 140 °C) can contribute a 19% (70% *vs.* 83%) increase in the digestibility of EA-ACP. A further increase in the temperature (140 to 160 °C) and a lower retention time (3 h *vs.* 1 h) resulted in a slight decrease in the yields of glucose and xylose. An increased pretreatment time appeared to have a positive effect on sugar release during enzymatic hydrolysis (at 140 °C: 73% for 1 h, 77% for 2 h and 83% for 3 h). Overall, pretreatment temperature and time have significant effects on sugar release. The optimized pretreatment condition was determined to be 20 wt% biomass loading, 140 °C and 3 h of pretreatment time, which resulted in over 80% sugar release. In general, the inhibition of enzyme activity and microbial toxicity of many ILs that are effective at biomass pretreatment (*e.g.* imidazolium-based ILs: [C_2C_1Im][OAc]) complicate downstream processing as they require excessive water wash to remove residual IL from pretreated slurry prior to saccharification.[25–27] PILs are compatible with commercial enzymes (*e.g.* Novozymes Cellic®) at 5–10 wt% in water, so they can potentially be used in a one-pot process.[8,19] Fig. 4C

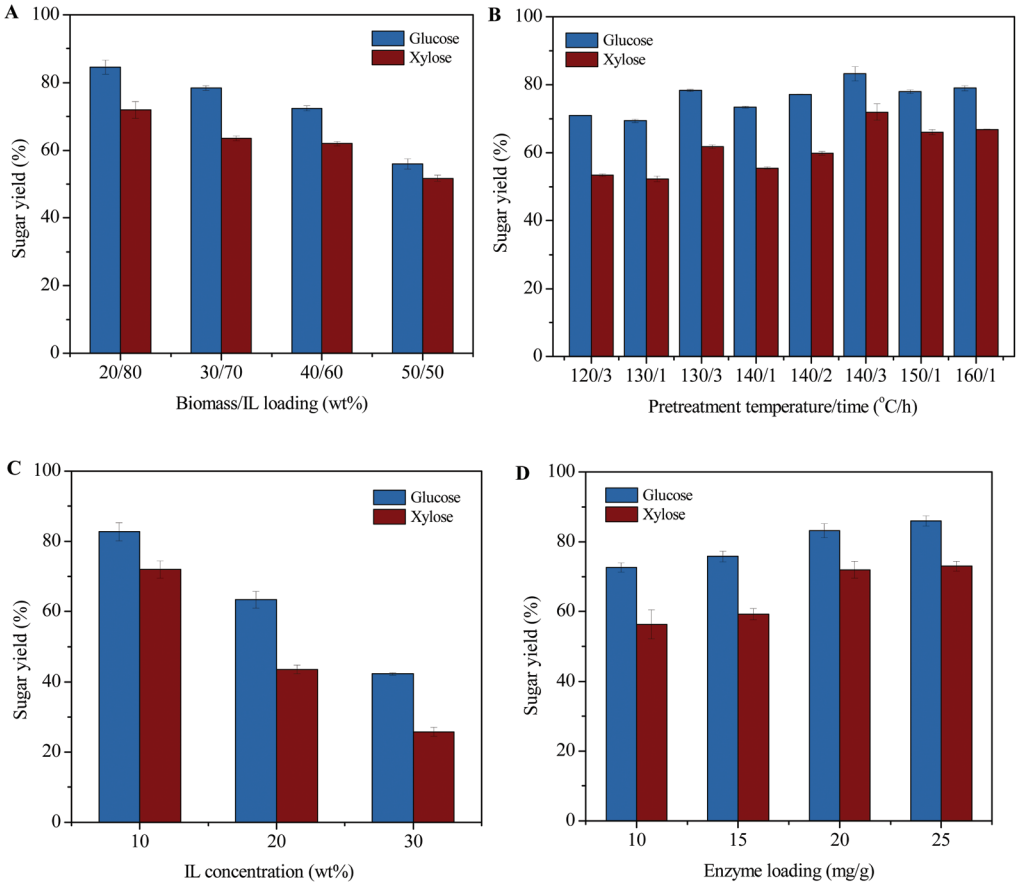

Fig. 4 Effects of some parameters on sugar yield: (A) biomass/IL loading; (B) pretreatment temperature/time; (C) IL concentration in saccharification; (D) enzyme loading. Conditions: pretreatment, 20 wt% ACP loading, 80 wt% IL, 140 °C, 3 h; saccharification, 10 wt% IL, 20 mg protein per g ACP, 50 °C, 72 h.

presents the effect of IL loading during enzymatic hydrolysis on the sugars release. A stepwise decrease in sugar yield was observed with the PIL loading increasing from 10 to 30 wt%. Therefore, 10 wt% of PIL appears to be the maximum concentration that permits function of hydrolytic enzyme mixtures. We have also investigated the effect of enzyme loading on monomeric sugar release (Fig. 4D). EA-ACP pretreated (140 °C and 3 h) biomass becomes more digestible at higher enzyme loadings. However, a glucose yield of 73% could still be achieved at 10 wt% of enzyme loading, indicating that the EA-ACP substrate is more susceptible to enzymatic hydrolysis. Overall, the EA-ACP optimized process parameters to achieve the maximum amount of sugars are 20/80 biomass to IL loading, 140 °C temperature, 3 h of time, 10 wt% of IL loading during enzymatic hydrolysis and 20 mg of enzyme loading.

To gain insights into the potential benefits of acid-IL pretreatment on enzymatic hydrolysis, it is necessary to assess EA-ACP under industrially relevant conditions. Thus, EA-ACP pretreated biomass under the optimal conditions was subjected to enzymatic hydrolysis at both 10 wt% and 20 wt% solids loading for 72 h (Fig. 5). Saccharification can suffer from poor mass/heat transfer at high solid loadings, which could limit the enzymatic polysaccharide deconstruction.[3] In

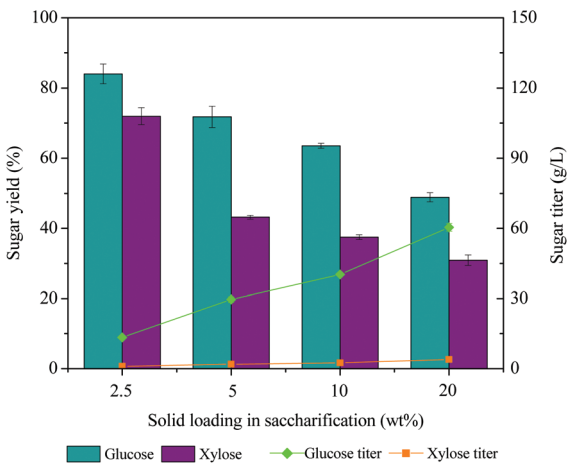

Fig. 5 Effects of solid loading in saccharification on sugar yield. Conditions: pretreatment, 20 wt% ACP loading, 80 wt% IL, 140 °C, 3 h; saccharification, 10 wt% IL, 20 mg protein per g ACP, 50 °C, 72 h.

the case of 5 wt% solid loading, a glucose yield of 73.9% still can be observed. However, increasing the solid loading from 10 wt% to 20 wt% decreased the glucose yield from 63.5% to 49.8% due to the water constraint. However, a glucose titer of

over 60 g L^{-1} from poplar biomass at 20 wt% of enzymatic solid loading was achieved using a consolidated one-pot process, which is an acceptable sugar titer for microbial conversion. Taken together, this data shows the effectiveness of a combined acid-IL pretreatment and suggests a possible route for one-pot microbial conversion to biofuels.

2.3 Compositional and structural changes during consolidated process

To determine the efficacy of each solvent, changes in cellulose (glucan), hemicellulose (xylan) and lignin (sum of acid soluble lignin and klason lignin) were tracked before and after pretreatment. Chemical composition, solid recovery, and component removal from the biomass after pretreatment with HAc and [EOA][OAc] at different temperatures are summarized in Table 1. Since IL decomposition occurs under higher temperature, lower temperature pretreatment condition is recommended (140 °C *vs.* 150–160 °C).[9] After pretreatment, 58–79 wt% of the solid residue was recovered, depending on the solvent, pretreatment temperature, and time. Generally, the consolidated pretreatment with HAc-PIL resulted in lower solid recovery (individual process = 74–79% *vs.* consolidated process = 58–60%). Also, pretreatment at higher temperatures led to lower solid recovery. After pretreatment by the individual or consolidated solvents, the glucan content was typically increased, and the use of PIL enabled higher glucan dissolution (10–15%) compared to that of HAc (0.4%). A large amount of xylan (~80%) was removed after HAc catalysis, indicating that HAc is an effective solvent on xylan degradation. Moreover, xylan content was decreased from 4.9% to 3.6% and a ~88% removal was achieved with the addition of PIL in the consolidated process. Further, it is also interesting to note that the PIL pretreatment facilitated lignin removal (HAc treated = 17% *vs.* HAc–[EOA][OAc] treated = 33–46%). However, an individual PIL pretreatment alone is not sufficient to remove high amounts of xylan or lignin, which is likely caused by different inherent structural characteristics of wood compared to that of grasses.

Sun *et al.* studied the pretreatment of switchgrass using [EOA][OAc]. They reported that [EOA][OAc] is more effective in removing the lignin from biomass, almost 60% of lignin was removed at 140 °C for 3 h (10% biomass loading).[8] In our case, we have removed only 35% of lignin at similar conditions. Zhou *et al.* reported that 71% of lignin, 29.2% of hemicellulose, and 5.8% of cellulose were removed after the pretreatment of *Miscanthus x giganteus* using [EOA][OAc] at 120 °C for 10 h.[18] Whereas in our case, 35.2% of lignin, 29.7% of hemicellulose, and 11% of cellulose were removed at 140 °C for 3 h. The difference in the delignification effectiveness might be dependent on three aspects: (1) the biomass loading during the pretreatment, higher solid loading results in lower delignification due to the limitation of interactions between biomass and IL, (2) the pretreatment processes generally utilize the higher temperature or time, resulting in the effective solubilization of lignin, (3) finally, the amount and degree of biomass recalcitrance differ as a consequence of the biomass itself (*i.e.*, hardwood, softwood, and grass), and also is affected by intrinsic characteristics such as age, harvest methodology, the extent of drying, and storage conditions.

To evaluate the structural changes in the biomass that occur during HAc-PIL pretreatment, powder X-ray diffraction (PXRD) and thermogravimetric analysis (TGA/DTG) were performed to determine the crystallinity and thermal decomposition temperature of the poplar samples. The PXRD spectrum reveals the changes between crystalline cellulose and amorphous cellulose, hemicellulose, and lignin, which is generally expressed as crystallinity index (CrI) (Fig. 6). All poplar samples pretreated with HAc, [EOA][OAc] and HAc–[EOA][OAc] display

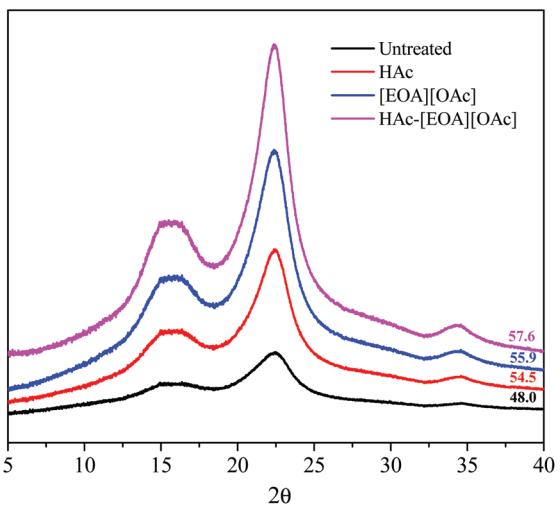

Fig. 6 X-ray diffraction patterns and CrI (%) value (noted on the right side of each spectrum) of poplar biomass before and after pretreatment.

Table 1 Compositional analysis after HAc, [EOA][OAc], and the consolidated pretreatment

Pretreatment Solvent	T/t (°C h^{-1})	Solid recovery (%)	Composition of pretreated biomass (%)			Removal after pretreatment (%)		
			Glucan	Xylan	Lignin	Glucan	Xylan	Lignin
—	—	—	43.3 ± 1.5	17.6 ± 2.5	27.8 ± 2.4			
HAc	170/0.5	74.0 ± 4.7	58.3 ± 2.4	4.9 ± 2.6	31.3 ± 1.6	0.4 ± 0.0	79.4 ± 2.6	16.7 ± 1.6
[EOA][OAc]	140/3	78.3 ± 4.1	49.2 ± 2.6	15.8 ± 1.9	23.0 ± 1.8	11.0 ± 2.6	29.7 ± 1.7	35.2 ± 1.5
HAc–[EOA][OAc]	170/0.5 + 140/3	57.9 ± 4.0	64.1 ± 1.9	3.7 ± 2.0	26.0 ± 2.3	14.3 ± 1.9	87.8 ± 2.0	45.8 ± 2.1
HAc–[EOA][OAc]	170/0.5 + 150/1	59.8 ± 3.2	64.9 ± 2.0	3.6 ± 1.8	31.0 ± 1.9	10.4 ± 0.9	87.8 ± 2.4	33.3 ± 1.1
HAc–[EOA][OAc]	170/0.5 + 160/1	58.1 ± 3.6	65.7 ± 1.3	3.6 ± 2.1	29.2 ± 2.2	11.8 ± 1.0	88.1 ± 1.8	39.0 ± 1.2

diffraction patterns characteristic of the cellulose I polymorph and are in semi-amorphous status with different degrees of crystallinity.[9] Poplar samples pretreated with different modes of solvents have increased CrI values relative to raw poplar (HAc: 54.5% < [EOA][OAc]: 55.9% < HAc–[EOA][OAc]: 57.6%). In our case, the driving factor that determines the crystallinity of pretreated solids is the removal of amorphous cellulose rather than the decrystallization of crystalline cellulose matrix. The increased CrI values point out that the removal of amorphous components is the leading role controlling pretreatment with HAc, [EOA][OAc] and HAc–[EOA][OAc], an obversion that is consistent with the composition analysis. After pretreatment with HAc, high hemicellulose removal and an increase in cellulose CrI are also in line with reports in the literature. Acid pretreatment can efficiently remove the hemicellulose but does not significantly alter the inter- and intra-molecular hydrogen bonds of cellulose.[22,28]

It is worthwhile to mention that, in the case of the imidazolium-based cation with acetate anion ([C_2C_1Im][OAc] and [C_4C_1Im][OAc]), the crystallinity of biomass was reduced and the structure of cellulose was changed from cellulose I (2θ = 22.4) to cellulose II (2θ = 20.2).[22,29] However, in our case with acetate-based PIL, the crystallinity of cellulose in both [EOA][OAc] and HAc–[EOA][OAc] was found to be increased, implying that recovered residual biomass showed cellulose type-I structure. This phenomenon could be explained by the fact that [EOA][OAc] is more efficient in lignin removal but not in altering the cellulose structure. On the other hand, the proton transfer in PIL (especially in acetic acid-based IL) is incomplete, resulting in the presence of neutral species as well. Moreover, the interaction energy between anion/cation in PIL ([EOA][OAc]) is much stronger than the aprotic ILs ([C_2C_1Im][OAc] and [C_4C_1Im][OAc]), which could control the interaction between cellulose and PIL (Table S1†). This suggests that interactions of anion/cation competing with the interactions of cellulose and PIL, resulting in the increased cellulose crystallinity.

The TGA and DTG curves of original poplar and pretreated solid residues are shown in Fig. 7. The weight loss below 120 °C was considered as the evaporation of moisture and volatile content in samples and major decomposition occurring from 150 °C to 790 °C.[30] Besides, there were still about 16–22 wt% of solid residues left after pyrolysis at 600 °C (Fig. 7A). According to the literature reports, hemicellulose, cellulose, and lignin decomposition occurred at 220–315 °C, 300–400 °C and 300–500 °C, respectively.[31,32] From Fig. 7, it was seen that the decomposition of poplar exhibited in two different stages. First, the curve of biomass showed one broad peak with a shoulder at the low temperature (200–280 °C) side.[33–35] This small shoulder was due to the occurrence of hemicellulose decomposition. While the second stage corresponds to 280–380 °C, which accounts for the thermal decomposition of cellulose and trace amounts of hemicellulose and lignin. As shown in Fig. 7B, it was clear that the first decomposition peak corresponding to the hemicellulose almost completely disappeared after the catalytic process of HAc (b and d curves), while cellulose and lignin component stay mainly retained. The disappearance of hemicellulose peak

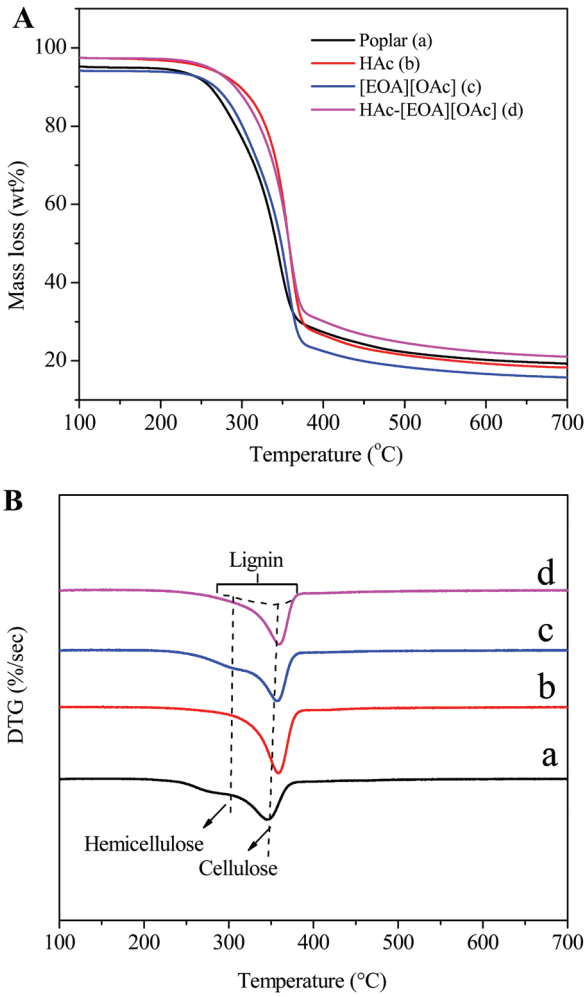

Fig. 7 TGA (A) and DTG (B) analysis of raw poplar and poplar samples pretreated with HAc, [EOA][OAc], and HAc–[EOA][OAc].

after the HAc catalytic process is due to the high extent of hemicellulose removal during acid pretreatment, observations that agree with the literature.[22] The hemicellulose fraction in solid residues pretreated with PIL lessened, but most of the hemicellulose remained within the poplar, which was consistent with the compositional data. The pyrolysis residue of poplar decreased sharply when acid-IL was performed. The decrease in pyrolysis samples could be mainly attributed to the removal of hemicellulose, lignin and the reduced amount of ash.[36] In the case of lignin, it normally produces more char than holocellulose during pyrolysis.[37] When examining the DTG curves, a peak at 345 °C was observed in the untreated raw poplar, while the pretreated sample had peaks that were >345 °C. This increase in thermal stability of cellulose corresponds to the higher crystallinity of recovered residual samples and the results are in agreement with the PXRD.

The mass balance of the HAc catalysis and one-pot PIL pretreatment and saccharification is displayed in Fig. 8. During the HAc catalysis, the majority of xylan was solubilized as xylooligosaccharides and xylose. After the one-pot PIL pretreatment and saccharification, a high amount of glucose (39.0 g)

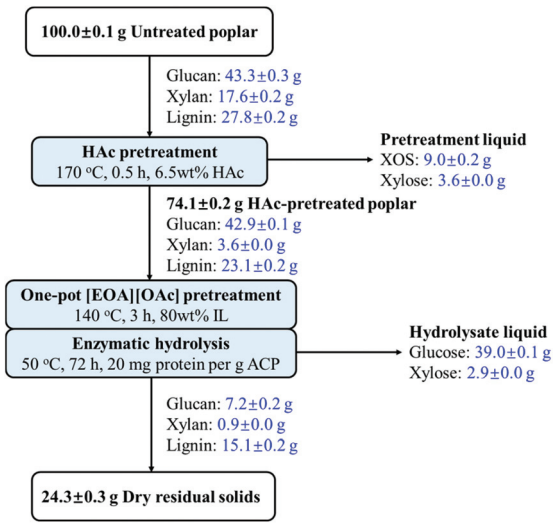

Fig. 8 Mass balance on the HAc catalysis and one-pot PIL configuration.

was liberated from the HAc-pretreated solids and only 24.3 g of dry solids remained, mainly consisting of lignin. Taken together, the proposed strategy for conversion of poplar polysaccharides generates 9.0 g xylooligosaccharides, 6.5 g xylose and 39.0 g glucose, which are 83.6% and 81.8% of the poplar xylan and glucan, respectively.

2.4 Understanding the solvent effects on poplar pretreatment by molecular simulations

To understand the thermodynamic effects of investigated solvents on the removal of cellulose, hemicellulose, and lignin during the biomass pretreatment, molecular simulations were carried out to study the interactions. Table 2 reports the COSMO-RS predicted total excess enthalpy (H^E) and its energetic contributions to the biomass–HAc (6.5%) system. The excess enthalpy is a useful thermodynamic property for measuring the difference in the strength of interactions between unlike species (*i.e.*, biomass-solvents). From Table 2, the excess enthalpy of cellulose, hemicellulose, and lignin with HAc/water mixture is exothermic, as indicated by the negative values of H^E. The H^E between hemicellulose and HAc/water mixtures is stronger than that of the cellulose and lignin which leads to the higher removal of hemicellulose during the HAc pretreatment. Further, a close look at the excess enthalpy contributors (Table 2), the higher hemicellulose removal occurred is due to the strong contribution from hydrogen bonding and electrostatic misfit interactions.

Alternatively, the higher removal of hemicellulose in HAc pretreatment can also be explained using Hansen Solubility Parameters (HSP). The principle of the solubility parameter is "like-dissolves-like". If solubility parameters of solvent and solute are similar, then the solubility of the solute in the solvent is predicted to be higher. As expected, the polar (δ_p) and hydrogen-bonded (δ_h) solubility parameters of HAc and hemicellulose are similar, conforming that the dominating interactions from hydrogen-bonding and electrostatic interactions (Table 3).

In the case of [EOA][OAc] pretreatment, the removal of lignin is highest, followed by hemicellulose and cellulose. The higher removal of lignin in [EOA][OAc] could be explained by predicting the strength of interactions, activity coefficient, and solubility parameters. Table 4 reports the COSMO-RS predicted

Table 2 COSMO-RS predicted total excess enthalpy (H^E) and energetic contributions to the total excess enthalpy (H^E_{MF}, H^E_{HB}, and H^E_{vdW}) in the biomass-HAc (6.5 wt%)/water system at T = 298.15 K[a]

Biomass component	H^E (kJ mol^{-1})	H^E_{MF} (kJ mol^{-1})	H^E_{HB} (kJ mol^{-1})	H^E_{vdW} (kJ mol^{-1})
Cellulose	−1.537	0.066	−1.748	0.145
Hemicellulose	−2.075	−0.058	−2.174	0.157
Lignin	−1.260	0.182	−1.474	0.033

[a] In HAc/water system the mole fraction of HAc is 0.065 and water is 0.935.

Table 3 Solubility parameters of biomass components and IL. The listed HSPs include various contributors' dispersion, polar, and hydrogen to the HSPs

Chemical name	δ_d	δ_p	δ_h	δ_t	Predicted model
Cellulose $(C_6H_{11}O_5)_n$	26.1	7.9	17.3	32.29	HSPiP
Hemicellulose $(C_5H_8O_4)_n$	25.4	7.4	15.5	30.66	HSPiP
Lignin	21.8	5.4	10.2	24.67	HSPiP
	16.7	13.5	11.3	24.30	Thielemans and Wool[38]
	21.9	14.1	16.9	31.05	Charles M. Hansen[39]
[EOA][Ac]	17.02	38.42[a]		42.02	MD simulations
Ethanolamine	17	15.5	21	31.15	HSPiP
HAc	14.5	8	13.5	21.37	HSPiP
[EOA] + [HAc][b]	15.75	11.75	17.25	26.15	HSPiP

[a] δ_e is the HSP contribution from electrostatic term $\delta_e = \sqrt{(\delta_p^2 + \delta_h^2)}$. [b] [EOA] + [HAc] = $x_{[EOA]}$ = 0.5 and $x_{[HAc]}$ = 0.5.

Table 4 COSMO-RS predicted total excess enthalpy (H^E) and logarithmic activity coefficient (ln(γ)) of the biomass-[EOA][OAc] and [EOA] + [HAc] systems at T = 298.15 K[a]

	H^E (kJ mol^{-1})		ln(γ)	
Biomass component	[EOA] + [HAc]	[EOA][OAc]	[EOA] + [HAc]	[EOA][OAc]
Cellulose	−0.950	−4.734	−0.439	1.387
Hemicellulose	−0.254	−3.632	−0.362	2.294
Lignin	−0.278	−8.731	−0.617	1.386

[a] In [EOA][OAc] system the mole fraction of cation is 0.5 and anion is 0.5, and in the neutral species: the mole fractions of [EOA] and [HAc] are 0.5 and 0.5, respectively.

excess enthalpy and logarithmic activity coefficient (ln(γ)) of cellulose, hemicellulose and lignin in ionic and neutral species of PIL. The activity coefficient values are often used as a quantitative descriptor for the dissolution power of a solvent. In the literature, it has been reported that the activity coefficient was the dominating parameter in deciding the capability of solvents and was also successfully employed in previous works on the cellulose solubility in ILs.[40,41] Later studies reported that both excess enthalpy and activity coefficient parameters have significant effects on cellulose and lignin solubility.[42–44] Therefore, in the present work, we calculated both H^E and ln(γ) parameters to study their effects on biomass solubility.

It is important to stress that in protic ionic liquids (PILs), the proton transfer from the acid to the base leads to the presence of individual anions and cations.[11,45,46] However, in reality, various factors govern the proton transfer and the complete proton transfer is highly unlikely, which results in the presence of both ionic and neutral species in the solvent.[47–49] In the case of [EOA][OAc], the favorability of proton transfer was computed by quantum chemical simulations and we found that the proton transfer is incomplete, which suggests that the neutral species is indeed present in the mixture (see ESI Table S1†). It is also reported that the proton transfer is less likely to occur between a weaker acid and a primary amine.[50,51]

Moreover, the difference between the proton affinity of HAc (342.33 kcal mol^{-1}) and ethanolamine (220.87 kcal mol^{-1}) is large. The larger difference in proton affinities, the lower possibility of proton transfer between acid and base.[52,53] Thus, this study also investigated the effects of neutral species on biomass pretreatment. From Table 4, the excess enthalpy of biomass components in both [EOA][OAc] and its neutral species are displaying exothermic behavior, indicating the stronger interaction between biomass components and PIL species. Whereas in the case of ln(γ), the activity coefficients of lignin in the neutral species of PIL are predicted to be more negative, signifying the higher solubility of lignin. The fact can also be further explained by Hansen solubility parameters (HSP). The HSP value of neutral species of [EOA][OAc] is close to the lignin which resulted in lower activity coefficients and higher removal of lignin (Tables 3 and 4). Therefore, an excess enthalpy, ln(γ), and HSP parameters present similar bias with exothermic behavior of the mixtures, low ln(γ), and closer HSP values of their components related to the high solubility of lignin. Moreover, the contribution from both PIL and its neutral species has significant effects on the biomass pretreatment, especially on lignin removal. It is worthwhile to mention that in general, the predicted interactions of solutes are not comparable due to different substances have different free energy of fusion. However, the present molecular simulation results agree well with the experimental observations.

3. Conclusions

Many traditional pretreatment solvents are difficult to recycle or have inconsistent efficiency on softwoods and hardwoods due to their more recalcitrant cell walls compared to herbaceous feedstocks. To compete with traditional biorefineries, an innovative process needs to be developed that uses recyclable catalysts that can enable high-efficiency lignocellulose deconstruction. We demonstrated an integrated acetic acid based one-pot protic ionic liquid pretreatment and saccharification for the production of value-added hemicellulose-derived chemicals and fermentable sugars from poplar. This unprecedented conversion technology was centered around two recoverable and low-cost chemicals: acetic acid (HAc) and ethanolamine acetate ([EOA][OAc]). HAc is a widely available, inexpensive commodity chemical that enables easy recycling *via* vacuum distillation or liquid–liquid extraction in the first step of our process, and can then be used in the next step in the process as the anion in [EOA][OAc]. The cation ethanolamine is also a cheap and commercially available chemical. In addition, one of the motivations for [EOA][OAc] selection is the ability to recover and recycle this protic IL. The recyclability of protic ILs has been widely investigated and demonstrated for over a decade.[54] The efficiency of IL distillation has been investigated and addressed to be dependent upon the relative basicity of the competing bases (EOA and acetate in the present case). Another motivation for [EOA][OAc] selection is to avoid the need for intermediate pH adjustment and water-wash steps, enabling a one-pot process. Under optimized conditions, a glucose yield of over 80% was achieved. The high hemicellulose removal effect of HAc and the excellent delignification by [EOA][OAc] are the critical contributors to the high

pretreatment efficiency of woody biomass. However, a water-wash step was determined to be the essential prior to one-pot IL pretreatment on HAc-pretreated feedstock due to the role of water as an anti-solvent. It should be clarified that after the dilution of PIL pretreated solids, no degradation products derived from glucose or xylose were detected. We also studied the mechanism of biomass pretreatment in HAc and [EOA][OAc] by employing molecular simulations, such as COSMO-RS model and Hansen solubility parameters. We also estimated the proton transfer favorability between acid and base in [EOA][OAc] using quantum chemical calculations and it was found that the proton transfer is incomplete, suggesting that the neutral species is also present in this solvent. The strong interaction energy, lower activity coefficient, and close Hansen solubility parameters we determined in this study help us understand the mechanism that drives the high delignification observed by [EOA][OAc]. Moreover, we found that the energetic contribution from both ionic and neutral species of [EOA][OAc] has significant effects on the biomass pretreatment. The application of this predictive tool and the insights gained here will assist in developing subsequent novel protic ionic liquids for biomass pretreatment. Overall, after further optimization of the process outlined in this study, it will be possible to achieve the near full conversion of polysaccharides from woody biomass to several different valuable products using green and low-cost solvents under mild processing conditions.

4. Experimental section

4.1 Materials

In the present study, poplar biomass was used as the feedstock and acquired from Jiangsu province in China. The biomass samples were ground using a Thomas-Wiley® Mill fitted with a 2 mm sieve and then pass through a 20-mesh size screen (<0.85 mm). Thereafter, the samples were then stored at room temperature in a sealed plastic bag. Commercial enzyme cocktails Cellic® CTec 3 and HTec 3 were kindly provided by Novozymes. Ethanolamine (≥99.0%), HAc (≥99.7%), dichloromethane (anhydrous, ≥99.8%) and ethanol were purchased from Sigma-Aldrich and used without further purification.

4.2 Preparation of [EOA][OAc]

[EOA][OAc] was prepared according to the procedure reported in the literature.[55] [EOA][OAc] was prepared by dropping 1 equivalent amount of HAc to the dichloromethane–ethanol solution of 1 equivalent of the ethanolamine at room temperature. After stirring for 2 h, the organic solvents were evaporated in the lyophilizer (−50 °C) and the residue was dried in a vacuum oven at 50 °C for 48 h to generate the desired product. The structure of [EOA][OAc] was identified by the analysis of their ^{1}H NMR spectra (Fig. S1†). Further, the thermal properties (heat of fusion) and stability of PIL were measured by TGA/DSC instruments. The DSC curve showed that the melting temperature (T_m) which was taken as the onset of an endothermic peak on heating is 67 °C, and the heat of fusion is 14 625.84 J mol^{-1}. Fig. S1† showed the weight loss and thermal behavior of synthesized PIL. [EOA][OAc] showed a rapid weight loss between 120 and 200 °C, which corresponds to the thermal degradation of the PIL. Moreover, the TGA of [EOA][OAc] was verified with the literature TGA/DTG curve.[18]

4.3 Consolidated biomass pretreatment and enzymatic hydrolysis

HAc catalytic hydrolysis. The 75 mL Parr 5000 Multi-Reactor system (Parr Instrument Company, Moline, IL, USA) was used for HAc catalytic hydrolysis, which is equipped with six reactors with individual temperature/pressure monitoring and controlled by a flexible software. HAc catalytic hydrolysis parameters were adapted from the optimized conditions introduced by Huang *et al.*[6] The hydrolysis vessels were loaded with 2.5 g of poplar and 25 mL of HAc/water solution with a certain concentration of HAc (*i.e.*, 6.5 wt%). Under a thoroughly mixed condition, the reaction vessels were heated to 170 °C for 0.5 h. The solids were again filtered and dried in the lyophilizer (−50 °C) for further use.

One-pot pretreatment and saccharification. Following HAc catalytic hydrolysis, a typical one-pot pretreatment procedure was conducted. For example, 0.1 g of HAc pretreated poplar sample was mixed with [EOA][OAc] at 20 wt% biomass loading and 80 wt% PIL in a 15 mL sealed pressure tube and the tube was submerged in an oil bath at 140 °C for 3 h. After IL pretreatment, the pretreated slurry was diluted with DI water to reach an acceptable IL concentration of 10 wt%. Enzymatic saccharification was performed at 50 °C for 72 h with constant agitation on an Enviro Genie SI-1200 rotator platform (Scientific Industries, Inc., Bohemia, NY). The loading of enzyme cocktails (9CTec3/HTec3, v/v) is 20 mg protein per g biomass. The sugar yield was calculated according to the following equations:

$$\text{Glucose yield}(\%) = \frac{\text{glucose}[g] \times 0.9}{\text{glucan}[g]\text{in HAc} - \text{pretreated solids}} \times 100 \quad (1)$$

$$\text{Xylose yield}(\%) = \frac{\text{xylose}[g] \times 0.88}{\text{xylan}[g]\text{in HAc} - \text{pretreated solids}} \times 100 \quad (2)$$

4.4 Analysis and characterization methods

Analytical methods by HPLC. The chemical compositions of all the poplar samples before and after hydrolysis/pretreatment were measured using the standard protocols developed by National Renewable Energy Laboratory (NREL).[56] Sugars were quantified by high performance liquid chromatography (Agilent HPLC 1200 Series) equipped with a Bio-Rad Aminex HPX-87H column and a refractive index detector. The equipment was operated at a flow rate of 0.6 mL min^{-1} and the column temperature was 60 °C using 4 mM H_2SO_4 as the mobile phase. For oligomers detection, an aliquot of 72%

H_2SO_4 was added into an equal volume aliquot of hydrolysate, incubated at 30 °C for 1 h. Then the aqueous fraction was diluted to 4% H_2SO_4 and autoclaved at 121 °C for 1 hour according to the NREL protocol.[57] The identification of peaks was confirmed by standard calibration plots (regression coefficient was 0.99).

Nuclear magnetic resonance (NMR). The synthesized [EOA][OAc] was analyzed by ^{1}H NMR (Bruker Advance-800 MHz instrument, Germany) to confirm the purity and presence of different constituents. For ^{1}H NMR analysis, IL sample (~10 mg) was placed in NMR tubes with 500 μL DMSO-*d*6 (Sigma-Aldrich, 99.96% purity) and properly sealed with a cap. The purity of the PIL was ascertained from the NMR spectra by comparing the hydrogen atom areas of acid and base, respectively. The purity calculation procedure is already reported elsewhere.[58] Chemical shifts were referenced to the central DMSO peak (δ_H = 2.50 ppm for ^{1}H).

Powder X-ray diffraction (PXRD). The crystallinity of poplar biomass before and after pretreatment was characterized by the powder X-ray diffraction (PXRD) method described by Sun *et al.*[8] The XRD patterns were collected in the 2θ range from 5 to 60° and an exposure time of 300 s. The crystallinity index (CI) was calculated based on the crystalline and amorphous peak according to the following equation:[59,60]

$$\mathrm{CI}\% = \frac{I_{002} - I_{\mathrm{am}}}{I_{002}} \times 100\% \quad (3)$$

Thermogravimetric and differential scanning calorimetry analysis (TGA/DSC). To analyze the thermal behavior of [EOA][OAc] and poplar samples before and after hydrolysis/pretreatment, TGA and DTG analysis were performed on a TGA/DSC 3+ thermogravimetric analyzer using a Star^e system equipped with STARe software (V16.10). Approximately 10 mg of sample was heated in a weighting alumina pan with the heating rates of 5 K min^{-1} from 25 °C to 800 °C and a flow rate of 50 mL min^{-1} under a nitrogen atmosphere. Further, we have also analyzed the phase transition (*i.e.*, melting point and heat of fusion) properties of [EOA][OAc] on a TGA/DSC 3+ instrument. The heat of fusion was determined by the integration of heat capacity (C_p) which is the function of heat flow with differential temperature (dT). Hence, the integral area of the melting curve that gives information about the heat of fusion.[61]

4.5 Computational details

Quantum chemical calculations. The structures of cellulose (DP = 5), hemicellulose (DP = 5), lignin (formula: $C_{113}H_{126}O_{40}$; M. wt = 2124.21 g mol^{-1}), acetic acid (HAc), ethanolamine (EOA), isolated ions, water, and the pairs of HAc/EOA and $[OAc]^-/[EOA]^+$ are drawn in the Avogadro freeware software.[62] Gaussian09 package was used to optimize the geometries of investigated molecules at B3LYP (Becke 3-parameter hybrid functional combined with the Lee–Yang–Parr correlation) theory and 6-311+G (d, p) basis set. Frequency calculations were also performed to verify the reasonability of the optimized structures and energy minima.[24,57,63] Further, to study the favorability of the proton transfer from acid to the base, we have optimized the geometries of pairs of HAc/EOA and $[OAc]^-/[EOA]^+$ at hybrid B3LYP function corrected for dispersion interaction using Grimme's dispersion with Becke–Johnson damping (GD3BJ) empirical term.[64–66] The B3LYP functional and Grimme's dispersion has been applied successfully and extensively used to study the structure and intermolecular interactions in the protic ionic liquids.[49,52,65,67,68] The cartesian coordinates of all the optimized structures along with their energy values were provided in the ESI.†

COSMO-RS calculations. The COSMO-RS calculations were carried out following multiple simulation steps. First, the geometries of all the investigated molecules were optimized using quantum chemical calculations and described in the above section. After geometry optimization, the next step is to generate the COSMO file using the BVP86/TZVP/DGA1 level of theory.[44,69,70] The combination of TZVP and DGA1 basis sets allows the electron density to adjust spatially to the extent appropriate to the particular molecular environment. The ideal screening charges on the molecular surface were then computed using the same level of theory BVP86 *via* the keyword "scrf = COSMORS".[71,72] The generated COSMO files were then used as the input in the COSMOtherm (version 19.0.1, COSMOlogic, Leverkusen, Germany) package.[73,74] BP_TZVP_19 parametrization was used to calculate the sigma profiles and sigma potentials of the isolated molecules, and excess enthalpy (H^E) and logarithmic activity coefficients (ln(γ)) of mixtures. In COSMO-RS calculations, the molar fraction of solute (cellulose, hemicellulose and lignin) is set to 0.2, whereas the molar fraction of solvent (acetic acid/water, [HAc] + [EOA], [EOA][OAc]) was set as 0.8. Therefore, the excess enthalpy (H^E) and logarithmic activity coefficients (ln(γ)) of mixtures were calculated accordingly.

The excess enthalpy of a mixture can be predicted by using the following eqn (4):[70]

$$H_M^E = \sum x_i H_i^E = \sum x_i [H_{(i,\mathrm{mixture})} - H_{(i,\mathrm{pure})}] \quad (4)$$

where, H_m^E is the excess enthalpy of each molecule in the mixture, defined as the enthalpy difference between component *i* in the mixture and in the pure state.

On the other hand, excess enthalpy of a mixture is an algebraic sum of three contributors (eqn (5)) associated with electrostatic misfit, hydrogen bonding and van der Waals forces.

$$H_M^E = H_M^E\ (\mathrm{misfit}) + H_M^E\ (\text{H-bond}) + H_M^E\ (\mathrm{vdW}) \quad (5)$$

And the activity coefficient of component *i* is related to the chemical potential μ_i is given as:[75]

$$\ln(\gamma_i) = \left(\frac{\mu_i - \mu_i^0}{RT}\right) \quad (6)$$

where μ_i^0 is the chemical potential of the pure component *i*, *R* is the real gas contact and *T* is the absolute temperature. The more details of COSMO-RS calculation in predicting the excess enthalpies and activity coefficients are provided in the COSMOtherm's user manual.[76]

It was known fact that polymeric structures *i.e.*, cellulose, hemicellulose, and lignin exhibit multiple configurations. However, there are several ways to represent a polymer with the COSMOtherm program package. It is only computationally feasible to model a molecule with a low degree of polymerization. To model a polymer in COSMO-RS calculations, the end group of the polymer (cellulose/hemicellulose) is deactivated using a function called "weight string", which allows for selectively switching on/off certain atoms within a COSMOfile. The weight string function has been widely applied to polymers (repeated unit molecules) in the literature. Kahlen *et al.*, Liu *et al.* and Casas *et al.* modeled mid-monomer of cellotriose and mid-dimer of cellotetraose to represent the cellulose model polymeric structure in COSMO-RS calculations to screen the hundreds of ionic liquids.[40,43,44] Further, Loschen and Klamt used mid-trimer of polyethylene glycol as a polyethylene glycol polymer structure.[77] Hence, the mid-dimer for cellulose and mid-trimer part for hemicellulose are obtained and used in the COSMO-RS calculations (Fig. S2†).

Calculation of solubility parameters. The solubility parameter of a solvent is one of the key parameters that measure the polarity and quantify the 'like-dissolves-like' principle, which is an important parameter in polymers dissolutions. The solubility parameters of investigating molecules were calculated by Hansen solubility parameters in practice (HSPiP) and molecular dynamics (MD) simulations. The molecular dynamics (MD) simulations were carried out only for IL ([EOA][OAc]), whereas the HSPiP tool was used for other chemical compounds. The MD simulations were performed with the NAMD package software at constant temperature (298.15 K) and pressure using Langevin thermostat and Nose–Hoover Langevin barista.[78–80] The CHAMRMM force filed parameters were employed.[81] The initial configuration of ionic pairs (800 molecules) of IL was prepared by PACKMOL in a cubic box and the bulk ionic box corresponds to the liquid phase. Initially, the simulated system energy was minimized for 1 ns.[82] Thereafter, the system was gradually heated to 298.15 K for 0.5 ns. At the desired temperature, the system was equilibrated under the NPT ensemble to get the system converge to its experimental condition for 8 ns. Subsequently, the production run lasted for 20 ns under constant NVT ensemble. From the final configuration of liquid phase simulations, three random ionic pairs were selected as an initial configuration for the gas phase simulations and the results were subsequently averaged over all the independent simulations. At every 5 ps, the production data was saved for computing the cohesive energy density (CED) and solubility parameter (δ) of the IL. The detailed information about the calculation of solubility parameters from MD simulations is provided elsewhere.[83,84]

Conflicts of interest

There are no conflicts of interests to declare.

Acknowledgements

The work was supported by the National Key R&D Program of China (2017YFD0601001). The authors also acknowledge the Priority Academic Program Development of Jiangsu Higher Education Institutions (PAPD) for supporting the work presented in this paper. This work was part of the DOE Joint BioEnergy Institute (http://www.jbei.org) supported by the U.S. Department of Energy, Office of Science, Office of Biological and Environmental Research, through contract DE-AC02-05CH11231 between Lawrence Berkeley National Laboratory and the U.S. Department of Energy. The views and opinions of the authors expressed herein do not necessarily state or reflect those of the United States Government or any agency thereof. Neither the United States Government nor any agency thereof, nor any of their employees, makes any warranty, expressed or implied, or assumes any legal liability or responsibility for the accuracy, completeness, or usefulness of any information, apparatus, product, or process disclosed or represents that its use would not infringe privately owned rights. The authors also acknowledge the work at the Molecular Foundry was supported by the Office of Science, Office of Basic Energy Sciences, of the U.S. Department of Energy under Contract no. DE-AC02-05CH11231. XRD characterization was conducted with the help of Dr Tevye Kuykendall at the Molecular Foundry in Lawrence Berkeley National Laboratory.

References

1 N. Mosier, C. Wyman, B. Dale, R. Elander, Y. Y. Lee, M. Holtzapple and M. Ladisch, *Bioresour. Technol.*, 2005, **96**, 673–686.
2 K. H. Kim, A. Eudes, K. Jeong, C. G. Yoo, C. S. Kim and A. Ragauskas, *Proc. Natl. Acad. Sci. U. S. A.*, 2019, **116**, 13816–13824.
3 F. Xu, J. Sun, N. V. S. N. M. Konda, J. Shi, T. Dutta, C. D. Scown, B. A. Simmons and S. Singh, *Energy Environ. Sci.*, 2016, **9**, 1042–1049.
4 C. E. Wyman, V. Balan, B. E. Dale, R. T. Elander, M. Falls, B. Hames, M. T. Holtzapple, M. R. Ladisch, Y. Y. Lee, N. Mosier, V. R. Pallapolu, J. Shi, S. R. Thomas and R. E. Warner, *Bioresour. Technol.*, 2011, **102**, 11052–11062.
5 K. X. Huang, J. Luo, Y. W. Wu and Y. Xu, *ACS Sustainable Chem. Eng.*, 2019, **7**, 2406–2413.
6 K. X. Huang, J. Luo, R. Cao, Y. Su and Y. Xu, *J. Wood Chem. Technol.*, 2018, **38**, 371–384.
7 L. Kumar, V. Arantes, R. Chandra and J. Saddler, *Bioresour. Technol.*, 2012, **103**, 201–208.
8 J. Sun, N. V. S. N. M. Konda, R. Parthasarathi, T. Dutta, M. Valiev, F. Xu, B. A. Simmons and S. Singh, *Green Chem.*, 2017, **19**, 3152–3163.
9 N. Sun, R. Parthasarathi, A. M. Socha, J. Shi, S. Zhang, V. Stavila, K. L. Sale, B. A. Simmons and S. Singh, *Green Chem.*, 2014, **16**, 2546–2557.

10 J. Sun, N. V. S. N. M. Konda, J. Shi, R. Parthasarathi, T. Dutta, F. Xu, C. D. Scown, B. A. Simmons and S. Singh, *Energy Environ. Sci.*, 2016, **9**, 2822–2834.
11 T. L. Greaves and C. J. Drummond, *Chem. Rev.*, 2008, **108**, 206–237.
12 J. E. Reid, F. Agapito, C. E. Bernardes, F. Martins, A. J. Walker, S. Shimizu and M. E. M. da Piedade, *Phys. Chem. Chem. Phys.*, 2017, **19**, 19928–19936.
13 C. Chiappe, A. Mezzetta, C. S. Pomelli, G. Iaquaniello, A. Gentile and B. Masciocchi, *Green Chem.*, 2016, **18**, 4982–4989.
14 G. F. De Gregorio, C. C. Weber, J. Grasvik, T. Welton, A. Brandt and J. P. Hallett, *Green Chem.*, 2016, **18**, 5456–5465.
15 D. W. Shang, X. P. Zhang, S. J. Zeng, K. Jiang, H. S. Gao, H. F. Dong, Q. Y. Yang and S. J. Zhang, *Green Chem.*, 2017, **19**, 937–945.
16 M. J. Earle, J. M. S. S. Esperanca, M. A. Gilea, J. N. C. Lopes, L. P. N. Rebelo, J. W. Magee, K. R. Seddon and J. A. Widegren, *Nature*, 2006, **439**, 831–834.
17 R. C. Remsing, R. P. Swatloski, R. D. Rogers and G. Moyna, *Chem. Commun.*, 2006, 1271–1273.
18 Q. Zhou, J. Chen, C. Wang, G. Yang, X. Ji, J. Peng and F. Xu, *Ind. Crops Prod.*, 2020, **147**, 112232.
19 B. Peric, J. Sierra, E. Marti, R. Cruanas, M. A. Garau, J. Arning, U. Bottin-Weber and S. Stolte, *J. Hazard. Mater.*, 2013, **261**, 99–105.
20 H. Y. Zhang, Y. Xu and S. Y. Yu, *Bioresour. Technol.*, 2017, **234**, 343–349.
21 A. A. N. Gunny, D. Arbain, R. E. Gumba, B. C. Jong and P. Jamal, *Bioresour. Technol.*, 2014, **155**, 177–181.
22 M. Mohan, N. N. Deshavath, T. Banerjee, V. V. Goud and V. V. Dasu, *Ind. Eng. Chem. Res.*, 2018, **57**, 10105–10117.
23 Y. L. Zhao, X. M. Liu, J. J. Wang and S. J. Zhang, *J. Phys. Chem. B*, 2013, **117**, 9042–9049.
24 M. Mohan, T. Banerjee and V. V. Goud, *ACS Omega*, 2018, **3**, 7358–7370.
25 J. Shi, J. M. Gladden, N. Sathitsuksanoh, P. Kambam, L. Sandoval, D. Mitra, S. Zhang, A. George, S. W. Singer, B. A. Simmons and S. Singh, *Green Chem.*, 2013, **15**, 2579–2589.
26 J. M. Gladden, M. Allgaier, C. S. Miller, T. C. Hazen, J. S. VanderGheynst, P. Hugenholtz, B. A. Simmons and S. W. Singer, *Appl. Environ. Microbiol.*, 2011, **77**, 5804–5812.
27 M. B. Turner, S. K. Spear, J. G. Huddleston, J. D. Holbrey and R. D. Rogers, *Green Chem.*, 2003, **5**, 443–447.
28 C. Li, B. Knierim, C. Manisseri, R. Arora, H. V. Scheller, M. Auer, K. P. Vogel, B. A. Simmons and S. Singh, *Bioresour. Technol.*, 2010, **101**, 4900–4906.
29 J. A. Perez-Pimienta, M. G. Lopez-Ortega, P. Varanasi, V. Stavila, G. Cheng, S. Singh and B. A. Simmons, *Bioresour. Technol.*, 2013, **127**, 18–24.
30 M. Davaritouchaee, W. C. Hiscox, E. Terrell, R. J. Mancini and a. S. Chen, *Green Chem.*, 2020, **22**, 1182–1197.
31 A. H. Meng, H. Zhou, L. Qin, Y. G. Zhang and Q. H. Li, *J. Anal. Appl. Pyrolysis*, 2013, **104**, 28–37.
32 C. C. Song, H. Q. Hu, S. W. Zhu, G. Wang and G. H. Chen, *Energy Fuels*, 2004, **18**, 90–96.
33 E. Biagini, F. Barontini and L. Tognotti, *Ind. Eng. Chem. Res.*, 2006, **45**, 4486–4493.
34 S. S. Idris, N. A. Rahman, K. Ismail, A. B. Alias, Z. A. Rashid and M. J. Aris, *Bioresour. Technol.*, 2010, **101**, 4584–4592.
35 Y. P. Luo, J. J. Fan, V. L. Budarin, C. W. Hu and J. H. Clark, *Green Chem.*, 2017, **19**, 4889–4899.
36 A. Q. Zheng, Z. L. Zhao, Z. Huang, K. Zhao, G. Q. Wei, L. Q. Jiang, X. B. Wang, F. He and H. B. Li, *Green Chem.*, 2015, **17**, 1167–1175.
37 T. T. Qu, W. J. Guo, L. H. Shen, J. Xiao and K. Zhao, *Ind. Eng. Chem. Res.*, 2011, **50**, 10424–10433.
38 W. Thielemans and R. P. Wool, *Biomacromolecules*, 2005, **6**, 1895–1905.
39 C. M. Hansen, *Hansen solubility parameters: a user's handbook*, CRC press, 2007.
40 J. Kahlen, K. Masuch and K. Leonhard, *Green Chem.*, 2010, **12**, 2172–2181.
41 M. Mohan, P. Viswanath, T. Banerjee and V. V. Goud, *Mol. Phys.*, 2018, **116**, 2108–2128.
42 A. Casas, J. Palomar, M. V. Alonso, M. Oliet, S. Omar and F. Rodriguez, *Ind. Crops Prod.*, 2012, **37**, 155–163.
43 A. Casas, S. Omar, J. Palomar, M. Oliet, M. V. Alonso and F. Rodriguez, *RSC Adv.*, 2013, **3**, 3453–3460.
44 Y.-R. Liu, K. Thomsen, Y. Nie, S.-J. Zhang and A. S. Meyer, *Green Chem.*, 2016, **18**, 6246–6254.
45 M. Yoshizawa, W. Xu and C. A. Angell, *J. Am. Chem. Soc.*, 2003, **125**, 15411–15419.
46 Y. Cui, J. Yin, C. Li, S. Li, A. Wang, G. Yang and Y. Jia, *Phys. Chem. Chem. Phys.*, 2016, **18**, 19731–19737.
47 S. K. Davidowski, F. Thompson, W. Huang, M. Hasani, S. A. Amin, C. A. Angell and J. L. Yarger, *J. Phys. Chem. B*, 2016, **120**, 4279–4285.
48 M. Shen, Y. Zhang, K. Chen, S. Che, J. Yao and H. Li, *J. Phys. Chem. B*, 2017, **121**, 1372–1376.
49 K. Low, S. Tan and E. I. Pas, *Front. Chem.*, 2019, **7**, 208.
50 K. Hiraoka, *Can. J. Chem.*, 1987, **65**, 1258–1261.
51 M. Mautner, *J. Am. Chem. Soc.*, 1984, **106**, 1257–1264.
52 I. V. Fedorova and L. P. Safonova, *J. Phys. Chem. A*, 2019, **123**, 293–300.
53 L. E. Shmukler, I. V. Fedorova, M. S. Gruzdev and L. P. Safonova, *J. Phys. Chem. B*, 2019, **123**, 10794–10806.
54 A. W. T. King, J. Asikkala, I. Mutikainen, P. Järvi and I. Kilpeläinen, *Angew. Chem., Int. Ed.*, 2011, **50**, 6301–6305.
55 D. Simijonovic, Z. D. Petrovic and V. P. Petrovic, *J. Mol. Liq.*, 2013, **179**, 98–103.
56 J. B. Sluiter, R. O. Ruiz, C. J. Scarlata, A. D. Sluiter and D. W. Templeton, *J. Agric. Food Chem.*, 2010, **58**, 9043–9053.
57 B. H. A. Sluiter, R. Ruiz, J. Sluiter, D. Templeton and D. Crocker, *Determination of Structural Carbohydrates and Lignin in Biomass*, 2011.
58 M. Mohan, P. K. Naik, T. Banerjee, V. V. Goud and S. Paul, *Fluid Phase Equilib.*, 2017, **448**, 168–177.

59 M. Mohan, R. Timung, N. N. Deshavath, T. Banerjee, V. V. Goud and V. V. Dasu, *RSC Adv.*, 2015, **5**, 103265–103275.
60 S. Kumar, R. Gupta, Y. Lee and R. B. Gupta, *Bioresour. Technol.*, 2010, **101**, 1337–1347.
61 M. Mohan, T. Banerjee and V. V. Goud, *Can. J. Chem. Eng.*, 2019, **97**, 1100–1106.
62 M. D. Hanwell, D. E. Curtis, D. C. Lonie, T. Vandermeersch, E. Zurek and G. R. Hutchison, *J. Cheminf.*, 2012, **4**, 17.
63 M. J. Frisch, G. W. Trucks, H. B. Schlegel, G. E. Scuseria, M. A. Robb, J. R. Cheeseman, G. Scalmani, V. Barone, G. A. Petersson, H. Nakatsuji, X. Li, M. Caricato, A. Marenich, J. Bloino, B. G. Janesko, R. Gomperts, B. Mennucci, H. P. Hratchian, J. V. Ortiz, A. F. Izmaylov, J. L. Sonnenberg, D. Williams-Young, F. Ding, F. Lipparini, F. Egidi, J. Goings, B. Peng, A. Petrone, T. Henderson, D. Ranasinghe, V. G. Zakrzewski, J. Gao, N. Rega, G. Zheng, W. Liang, M. Hada, M. Ehara, K. Toyota, R. Fukuda, J. Hasegawa, M. Ishida, T. Nakajima, Y. Honda, O. Kitao, H. Nakai, T. Vreven, K. Throssell, J. A. Montgomery Jr., J. E. Peralta, F. Ogliaro, M. J. Bearpark, J. J. Heyd, E. N. Brothers, K. N. Kudin, V. N. Staroverov, T. A. Keith, R. Kobayashi, J. Normand, K. Raghavachari, A. P. Rendell, J. C. Burant, S. S. Iyengar, J. Tomasi, M. Cossi, J. M. Millam, M. Klene, C. Adamo, R. Cammi, J. W. Ochterski, R. L. Martin, K. Morokuma, O. Farkas, J. B. Foresman and D. J. Fox, *Gaussian 09 Rev. D.01*, Gaussian, Inc., Wallingford, CT, 2009.
64 X. Gonze, J.-P. Michenaud and J.-P. Vigneron, *Phys. Scr.*, 1988, **37**, 785.
65 I. V. Fedorova, M. A. Krestyaninov and L. P. Safonova, *J. Phys. Chem. A*, 2017, **121**, 7675–7683.
66 S. Grimme, S. Ehrlich and L. Goerigk, *J. Comput. Chem.*, 2011, **32**, 1456–1465.
67 I. V. Fedorova and L. P. Safonova, *J. Phys. Chem. A*, 2019, **123**, 3735–3742.
68 N. Chipanina, T. Aksamentova, S. Adamovich, A. Albanov, A. Mirskova, R. Mirskov and M. Voronkov, *Comput. Theor. Chem.*, 2012, **985**, 36–45.
69 M. Mohan, T. Banerjee and V. V. Goud, *J. Chem. Eng. Data*, 2016, **61**, 2923–2932.
70 M. Gonzalez-Miquel, M. Massel, A. DeSilva, J. Palomar, F. Rodriguez and J. F. Brennecke, *J. Phys. Chem. B*, 2014, **118**, 11512–11522.
71 M. Mohan, V. V. Goud and T. Banerjee, *Fluid Phase Equilib.*, 2015, **395**, 33–43.
72 R. Anantharaj and T. Banerjee, *Ind. Eng. Chem. Res.*, 2010, **49**, 8705–8725.
73 Y. Y. Li and Y. Y. Jin, *Renewable Energy*, 2015, **77**, 550–557.
74 F. Eckert and A. Klamt, *AIChE J.*, 2002, **48**, 369–385.
75 K. A. Kurnia, S. o. P. Pinho and J. o. A. Coutinho, *Ind. Eng. Chem. Res.*, 2014, **53**, 12466–12475.
76 F. Eckert and A. Klamt, *COSMOtherm, version C3.0 release 19.0.1, C3.0 release 19.0.1 ed*, COSMOlogic GmbH & Co KG, Leverkusen, Germany, 2019.
77 C. Loschen and A. Klamt, *Ind. Eng. Chem. Res.*, 2014, **53**, 11478–11487.
78 G. J. Martyna, D. J. Tobias and M. L. Klein, *J. Chem. Phys.*, 1994, **101**, 4177–4189.
79 S. E. Feller, Y. Zhang, R. W. Pastor and B. R. Brooks, *J. Chem. Phys.*, 1995, **103**, 4613–4621.
80 J. C. Phillips, R. Braun, W. Wang, J. Gumbart, E. Tajkhorshid, E. Villa, C. Chipot, R. D. Skeel, L. Kale and K. Schulten, *J. Comput. Chem.*, 2005, **26**, 1781–1802.
81 K. Vanommeslaeghe, E. Hatcher, C. Acharya, S. Kundu, S. Zhong, J. Shim, E. Darian, O. Guvench, P. Lopes and I. Vorobyov, *J. Comput. Chem.*, 2010, **31**, 671–690.
82 L. Martínez, R. Andrade, E. Birgin and J. Martínez, *J. Comput. Chem.*, 2009, **30**, 2157–2164.
83 J. Gupta, C. Nunes, S. Vyas and S. Jonnalagadda, *J. Phys. Chem. B*, 2011, **115**, 2014–2023.
84 H. S. Salehi, M. Ramdin, O. A. Moultos and T. J. Vlugt, *Fluid Phase Equilib.*, 2019, **497**, 10–18.